OXFORD

SOT | Society of Toxicology
www.toxsci.oxfordjournals.org

TOXICOLOGICAL SCIENCES, 145(1), 2015, 157–168

doi: 10.1093/toxsci/kfv041
Advance Access Publication Date: February 17, 2015

Comparative Localization and Functional Activity of the Main Hepatobiliary Transporters in HepaRG Cells and Primary Human Hepatocytes

Pamela Bachour-El Azzi[*,†,‡,1], Ahmad Sharanek[*,†,1], Audrey Burban[*,†], Ruoya Li[§], Rémy Le Guével[¶], Ziad Abdel-Razzak[‡], Bruno Stieger[||], Christiane Guguen-Guillouzo[†], and André Guillouzo[*,†,2]

[*]Inserm UMR991, Foie, Métabolismes et Cancer, Rennes, France; [†]Université de Rennes 1, Rennes, France, [‡]Université Libanaise, EDST-PRASE and EDST-AZM-center-LBA3B, Beirut, Lebanon, [§]Biopredic International, Saint Grégoire, France, [¶]ImPACcell, SFR Biosit, Université de Rennes 1, Rennes, France and [||]Department of Clinical Pharmacology and Toxicology, University Hospital, Zurich, Switzerland

[1]These authors contributed equally to this work.
[2]To whom correspondence should be addressed at Inserm UMR 991, Faculté des Sciences Pharmaceutiques et Biologiques, 35043 Rennes Cedex, France. Fax: +33 223235385. E-mail: andre.guillouzo@univ-rennes1.fr.

ABSTRACT

The role of hepatobiliary transporters in drug-induced liver injury remains poorly understood. Various *in vivo* and *in vitro* biological approaches are currently used for studying hepatic transporters; however, appropriate localization and functional activity of these transporters are essential for normal biliary flow and drug transport. Human hepatocytes (HHs) are considered as the most suitable *in vitro* cell model but erratic availability and inter-donor functional variations limit their use. In this work, we aimed to compare localization of influx and efflux transporters and their functional activity in differentiated human HepaRG hepatocytes with fresh HHs in conventional (CCHH) and sandwich (SCHH) cultures. All tested influx and efflux transporters were correctly localized to canalicular [bile salt export pump (BSEP), multidrug resistance-associated protein 2 (MRP2), multidrug resistance protein 1 (MDR1), and MDR3] or basolateral [Na^+-taurocholate co-transporting polypeptide (NTCP) and MRP3] membrane domains and were functional in all models. Contrary to other transporters, NTCP and BSEP were less abundant and active in HepaRG cells, cellular uptake of taurocholate was 2.2- and 1.4-fold and bile excretion index 2.8- and 2.6-fold lower, than in SCHHs and CCHHs, respectively. However, when taurocholate canalicular efflux was evaluated in standard and divalent cation-free conditions in buffers or cell lysates, the difference between the three models did not exceed 9.3%. Interestingly, cell imaging showed higher bile canaliculi contraction/relaxation activity in HepaRG hepatocytes and larger bile canaliculi networks in SCHHs. Altogether, our results bring new insights in mechanisms involved in bile acids accumulation and excretion in HHs and suggest that HepaRG cells represent a suitable model for studying hepatobiliary transporters and drug-induced cholestasis.

Key words: hepatobiliary transporters; membrane localization; transporter activity; HepaRG hepatocytes; human hepatocytes

ABBREVIATIONS

BEI	bile excretion index
BSEP	bile salt export pump
CDFDA	5(6)-carboxy-2′,7′-dichlorofluorescein diacetate
CCHH	conventional cultured human hepatocyte
HH	human hepatocyte

JC-1	5,5′,6,6′-Tetrachloro-1,1′,3,3′-tetraethylbenzimidazolo carbocyanine iodide
MDR	multidrug resistance protein
MK571	5 -(3-(2-(7-Chloroquinolin-2-yl)ethenyl)phenyl)-8-dimethylcarbamyl-4,6-dithiaoctanoic acid sodium salt hydrate
MRP	multidrug resistance-associated protein
NTCP	Na^+-taurocholate co-transporting polypeptide
OATP	organic anion transporting polypeptide
PBS	phosphate buffered saline
SCHH	sandwich-cultured human hepatocyte
TCA	taurocholic acid.

Hepatocytes are highly polarized cells exhibiting specialized apical (canalicular) and sinusoidal (basolateral) domains. They import and export a variety of exogenous and endogenous substrates largely via membrane transporters that are divided into two major groups: influx transporters mediating cellular uptake of appropriate substrates and efflux transporters responsible for their excretion into bile canaliculi or blood (Giacomini *et al.*, 2010). Bile acids and drugs are their main substrates; 95% of bile acids secreted into bile are reabsorbed in the ileum, diffused across the enterocyte to the basolateral membrane, exported into portal blood circulation, extracted at the hepatocyte sinusoidal membrane, and re-secreted into bile contributing therefore to bile formation through the so-called entero-hepatic circulation (Hofmann, 1999).

Hepatic uptake of biliary constituents at the sinusoidal domain of hepatocytes is mediated by both sodium-dependent and independent mechanisms (Nathanson and Boyer, 1991). Although sodium-independent uptake of bile salts is carried by members of the organic anion transporting polypeptide family (OATPs/*SLCOs*), sodium-dependent uptake is mediated by the Na^+-taurocholate co-transporting polypeptide (NTCP/*SLC10A1*) that represents the most relevant uptake system. It accounts for the uptake of the major part of conjugated bile acids and less than half of unconjugated bile acids (Kullak-Ublick *et al.*, 2000; Meier and Stieger, 2002). Bile salts are then carried across the hepatocyte and secreted into bile via canalicular transporters. Canalicular transport of bile constituents is mainly mediated by ABC superfamily transporters: bile salt export pump (BSEP/*ABCB11*), multidrug resistance-associated protein 2 (MRP2/*ABCC2*), P-glycoprotein [multidrug resistance protein 1 (MDR1)/*ABCB1*], phospholipid flippase (MDR3/*ABCB4*), and breast cancer resistance protein (BCRP/ABCG2). Although BSEP exports monovalent bile salts and is responsible for bile salt-dependent flow, MRP2 excretes divalent bile salts, glutathione and its conjugates, generating therefore the major part of bile salt independent bile flow (Kullak-Ublick *et al.*, 2000). MDR1 has been shown to transport amphipathic organic cations, whereas MDR3 translocates phosphatidylcholine from the inner to the outer leaflet of the canalicular membrane (Lefebvre *et al.*, 2009). An alternative efflux system belonging to the MDR subfamily, represented by MRP3 and MRP4, is localized to the basolateral membrane domain and provides an alternative excretory route for bile constituents when their canalicular excretion is impaired (Trauner and Boyer, 2003).

Impairment of bile flow is called cholestasis and may be caused by a functional impairment of canalicular secretory processes, which in turn results in an intracellular accumulation of cholephilic compounds, such as bile salts (Trauner *et al.*, 1998). Intrahepatic cholestasis of pregnancy and drug-induced cholestasis are acquired forms of cholestasis (Pauli-Magnus *et al.*, 2010). Drug-induced cholestasis may lead to drug-induced liver injury in humans. In many cases of acquired forms of cholestasis, activity and cellular distribution of hepatobiliary transporters are altered. Other mechanisms, such as altered cell polarity as a consequence of mistargeting of intracellular transport vesicles, cytoskeletal modification, disrupted cell–cell junctions, or deregulated signaling pathways may be involved in acquired cholestasis (Trauner and Boyer, 2003). Finally, oxidative stress as a primary causative agent and/or as an aggravating factor has been linked to cholestatic liver injury (Anthérieu *et al.*, 2013; Copple *et al.*, 2010; Perez *et al.*, 2006; Roma and Sanchez Pozzi, 2008).

Although major progress has been made in the knowledge of transporters, their regulation and interactions with drugs and substrates, their role in drug-induced liver injury, in particular drug-induced cholestasis, requires further investigations (Corsini and Bortolini, 2013; Liu *et al.*, 2014). Various *in vivo* and *in vitro* biological approaches are currently used for studying hepatic transporters. Sandwich-cultured primary hepatocytes are considered as the most appropriate cell model to mimic the hepatobiliary secretory process (De Bruyn *et al.*, 2013); because major species differences have been reported in this process, the use of sandwich-cultured primary human hepatocytes (SCHHs) is desirable (Guguen-Guillouzo and Guillouzo, 2010; Swift *et al.*, 2010).

Recent studies have shown that cholestasis can be induced by drugs in human HepaRG cells, a human liver cell line expressing features of mature hepatocytes and exhibiting typical bile canaliculi. These findings suggest that HepaRG cells may be useful to mechanistically better understand drug-induced alterations of bile acids influx and efflux (Anthérieu *et al.*, 2013; Sharanek *et al.*, 2014). Whether the transport process in this cell model compares well with that in primary HHs in conventional or sandwich configuration remains currently unanswered. In this work, we showed that cellular localization and functional activity of the main hepatobiliary transporters were comparable in HepaRG cells and primary HHs.

MATERIALS AND METHODS

Reagents. Phalloidin fluoprobe was purchased from Interchim (Montluçon, France), [^{3}H]-taurocholic acid ([^{3}H]-TCA) was purchased from Perkin Elmer (Boston, Massachusetts), verapamil, 5 -(3-(2-(7-Chloroquinolin-2-yl)ethenyl)phenyl)-8-dimethylcarbamyl-4,6-dithiaoctanoic acid sodium salt hydrate (MK571) and 5(6)-carboxy-2′,7′-dichlorofluorescein diacetate (CDFDA) were purchased from Sigma (St Quentin Fallavier, France). 5,5′,6,6′-Tetrachloro-1,1′,3,3′-tetraethylbenzimidazolo carbocyanine iodide (JC-1 dye) was obtained from Invitrogen-Molecular probes (Saint Aubin, France). Hoechst dye was obtained from Promega (Madison, Wisconsin). All primary antibodies, except BSEP and NTCP antibodies (from Dr B. Stieger laboratory), were obtained from Abcam (Cambridge, United Kingdom). Secondary antibodies were obtained from Santa Cruz Biotechnology (Santa Cruz). All other reagents were obtained from Sigma.

Cell cultures. HepaRG cells were seeded at a density of 2.6×10^4 cells/cm^2 in Williams' E medium supplemented with 10% fetal bovine serum, 100 U/ml penicillin, 100 mg/ml streptomycin, 5 mg/ml insulin, 2 mM glutamine, and 50 mM hydrocortisone hemisuccinate. After 2 weeks, HepaRG cells were shifted to the same medium supplemented with 1.7% dimethyl sulfoxide

for 2 additional weeks to obtain confluent differentiated cultures. At that time, cultures contained equal proportions of hepatocyte-like and progenitors/primitive biliary-like cells (Cerec *et al.*, 2007).

HHs were obtained from Biopredic International (St Gregoire, France). They were isolated by collagenase perfusion of histologically normal liver fragments from 8 adult donors undergoing resection for primary and secondary tumors (Guguen-Guillouzo *et al.*, 1982). Primary cultures were obtained by hepatocyte seeding at a density of 1.5×10^5 cells/cm^2 onto collagen-precoated plates in Williams' E medium supplemented with 10% fetal bovine serum, 100 units/μl penicillin, 100 μg/ml streptomycin, 1 μg/ml insulin, 2 mM glutamine, and 1 μg/ml bovine serum albumin. The medium was discarded 12 h after cell seeding, and cultures were thereafter either maintained in the same medium as for HepaRG cells and designated as conventional cultured human hepatocytes (CCHHs), or after 24–48 h washed with cold medium and overlaid with matrigel at a concentration of 0.25 mg/ml in ice-cold Williams' E medium for the preparation of SCHHs. The medium of both CCHHs and SCHHs was renewed every day. CCHHs and SCHHs were prepared from the same donors and analyzed in parallel. SCHHs were used after at least 3-day matrigel overlay.

Immunolabeling. Cells were washed with warm phosphate buffered saline (PBS), fixed with either methanol for 15 min at −20°C or with 4% paraformaldehyde for 20 min at 4°C, and then washed three times with cold PBS. After paraformaldehyde fixation, cells were permeabilized for 20 min with 0.3% Triton in PBS followed by 1-h incubation in PBS containing 1% bovine serum albumin and 5% normal donkey serum. Cells were then incubated overnight with primary antibodies directed against NTCP (Kullak-Ublick *et al.*, 1997) and BSEP (Noe *et al.*, 2002) diluted at 1/200 and 1/50, respectively, MRP2 (M2III-6, Abcam) diluted at 1/100, MRP3 (M3II-9, Abcam), MDR1 (JSB-1, Abcam), or MDR3 (P3II-26, Abcam) diluted at 1/50 in PBS containing 1% bovine serum albumin and 5% normal donkey serum. After washing with cold PBS cells were incubated for 2 h with goat or rabbit Alexa fluor 488 labeled secondary antibodies in the same buffer as described earlier. Finally, cells were again washed with cold PBS and incubated with Hoechst and phalloidin in PBS for 20 min for F-actin and nuclei labeling, respectively. Immunofluorescence images were detected by Cellomics ArrayScan VTI HCS Reader (ThermoScientific, New Hampshire).

F-actin distribution. After fixation of cells as described earlier, cytoskeletal F-actin was localized using phalloidin fluoprobe SR101 (200 U/ml) diluted at 1/100 for 20 min as described previously (Pernelle *et al.*, 2011). Nuclei were labeled with 5 ng/ml Hoechst dye in parallel to F-actin labeling.

Functional activity of MDRs. The JC-1 metachromatic dye is translocated across the canalicular membrane via MDRs, particularly MDR1 (Legrand *et al.*, 2001). It does not accumulate in differentiated HepaRG hepatocytes without preincubation with verapamil, an inhibitor of MDRs (Pernelle *et al.*, 2011). Briefly, cells were incubated in the presence or absence of 50 μM verapamil (an inhibitor of MDRs) for 30 min, and then verapamil was washed out with warm PBS before 30 min incubation with 7 μM JC-1 at 37°C. Imaging was done by Cellomics ArrayScan VTI HCS Reader. Above a critical intracellular concentration, JC-1 forms dimers that display a specific red emission, whereas the monomers display a green emission.

NTCP activity. Activity of the NTCP transporter was measured through determination of radiolabeled TCA in cellular layers (cells plus bile canaliculi) (Anthérieu *et al.*, 2013). Briefly, HepaRG cells and 4–5 days CCHHs and SCHHs were washed twice with PBS and then incubated with [^{3}H]-TCA for 30 min in a buffer containing or not sodium ions. Cells were then washed twice with PBS and lysed with 0.1 N NaOH. Accumulation of the radiolabeled substrate in cellular layers was determined through scintillation counting.

Efflux of TCA. HepaRG cells and 4–5 days CCHHs and SCHHs were exposed to [^{3}H]-TCA for 30 min, and then washed with PBS. Efflux of radiolabeled TCA was assessed for 30 min in either standard or Ca^{2+}- and Mg^{2+}-free buffer. Cells were then scraped in 0.1 N NaOH and accumulation of radiolabeled substrate into cells + bile canaliculi (in the presence of Ca^{2+}- and Mg^{2+}-ions) and into cells only (in the absence of Ca^{2+}- and Mg^{2+}-ions) was measured through scintillation counting to evaluate TCA efflux. Absence of divalent cations promotes disruption of tight junctions and induces bile canaliculi opening (Liu *et al.*, 1999). This technology, called B-CLEAR technology, is patented and exclusively licensed to the Qualist Transporter Solutions Company, Durham, North Carolina.

To determine the contribution of passive diffusion to TCA efflux, cells were incubated in parallel in either standard or Ca^{2+}- and Mg^{2+}-free buffer for 30 min at 37°C or in standard buffer at 4°C after TCA uptake. Radiolabeled TCA was measured in all buffers and cells to calculate the relative contribution of diffusion and basolateral and canalicular efflux of TCA (Jemnitz *et al.*, 2010; Liu *et al.*, 1999; Marion *et al.*, 2012). Three different methods were used for calculation of efflux activity.

First, biliary excretion index (BEI) (method I), which represents the percentage of [^{3}H]-TCA that is excreted into bile canaliculi, was calculated using the following equation: $BEI = [(Accumulation_{Cells + Bile\ canaliculi} - Accumulation_{Cells})/Accumulation_{Cells + Bile\ canaliculi}] \times 100\%$ (Liu *et al.*, 1999).

The second method (method II) was based on the accumulation of TCA, after a 30-min efflux period, in cell lysates in the presence and absence of divalent cations (Liu *et al.*, 1999). Using TCA accumulation in cell lysates, diffusion, and basolateral and canalicular efflux were calculated using the following equations:

T_0=Total TCA uptake into the cell layer after 30 min incubation in standard buffer.

Total efflux = $T_0 - Accumulation_{Cells\ at\ 37°C}$.

Diffusion = $(T_0 - Accumulation_{Cells + Bile\ canaliculi\ at\ 4°C}) \times 100\%$/Total efflux.

The value "$T_0 - Accumulation_{Cells + Bile\ canaliculi\ at\ 4°C}$" represents the radiolabeled TCA that diffused out of cell layer.

Basolateral efflux = $[(T_0 - Accumulation_{Cells + Bile\ canaliculi\ at\ 37°C}) \times 100\%/Total\ efflux] - Diffusion$.

The value "$T_0 - Accumulation_{Cells + Bile\ canaliculi\ at\ 37°C}$" represents the radiolabeled TCA that is excreted in the medium either by basolateral transporters or by passive permeability.

Canalicular efflux = 100% − (Basolateral Efflux + diffusion).

The third method (method III) was based on radiolabeled TCA measured after a 30-min efflux period in standard and Ca^{2+}- and Mg^{2+}-free buffer (Jemnitz et al., 2010). Radioactivity in standard buffer at 37°C represented basolateral efflux and passive diffusion of TCA, whereas that in Ca^{2+}- and Mg^{2+}-free buffer corresponded to canalicular efflux in addition to basolateral efflux and passive diffusion.

Total efflux = Radioactivity in Ca^{2+} and Mg^{2+}-free buffer at 37°C.

Diffusion = Radioactivity in standard buffer at 4°C × 100%/Total efflux.

Basolateral efflux = (Radioactivity in standard buffer at 37°C – Radioactivity in standard buffer at 4°C) × 100%/Total efflux.

Canalicular efflux = (Radioactivity in Ca^{2+}- and Mg^{2+}-free buffer at 37°C – Radioactivity in standard buffer at 37°C) × 100%/Total efflux.

CDF excretion. Cells were washed with warm PBS, pre-incubated for 20 min in the presence or absence of 30 μM MK571, an inhibitor of MRP2, before addition of 2 μM CDFDA for 30 min at 37°C in either standard or Ca^{2+}- and Mg^{2+}-free buffer. Upon hydrolysis of CDFDA by intracellular esterases, CDF is secreted into the bile canaliculi by membrane transporters, particularly MRP2 (Zamek-Gliszczynski *et al.*, 2003). Cells were then washed with PBS, and imaging was done using inverted microscope Zeiss Axiovert 200 M and AxioCam MRm.

Time-lapse imaging. Phase-contrast images of HepaRG cells, CCHHs, and SCHHs were captured each minute, using time-lapse phase-contrast videomicroscopy. The inverted microscope Zeiss Axiovert 200 M was equipped with a thermostatic chamber (37°C and 5% CO_2) to maintain the cells under normal culture conditions. Images were captured by AxioCam MRm camera with a ×20 objective and the mosaic tool of the microscope, which enabled the automated acquisition of multi-image mosaics at the defined positions.

Statistical analysis. One-way ANOVA with Bonferroni's multiple comparison test (GraphPad Prism 6.00) was performed to compare data between the three cell models. Each value corresponded to the mean ± standard deviation (SD) of at least three independent experiments. Data were considered significantly different when $P < 0.05$.

RESULTS

HepaRG Cell and HH Polarity

Under phase-contrast microscopy, HepaRG hepatocytes and HHs either in conventional culture or in a sandwich configuration formed clusters with well-defined intercellular structures resembling characteristic bile canaliculi (Fig. 1A).

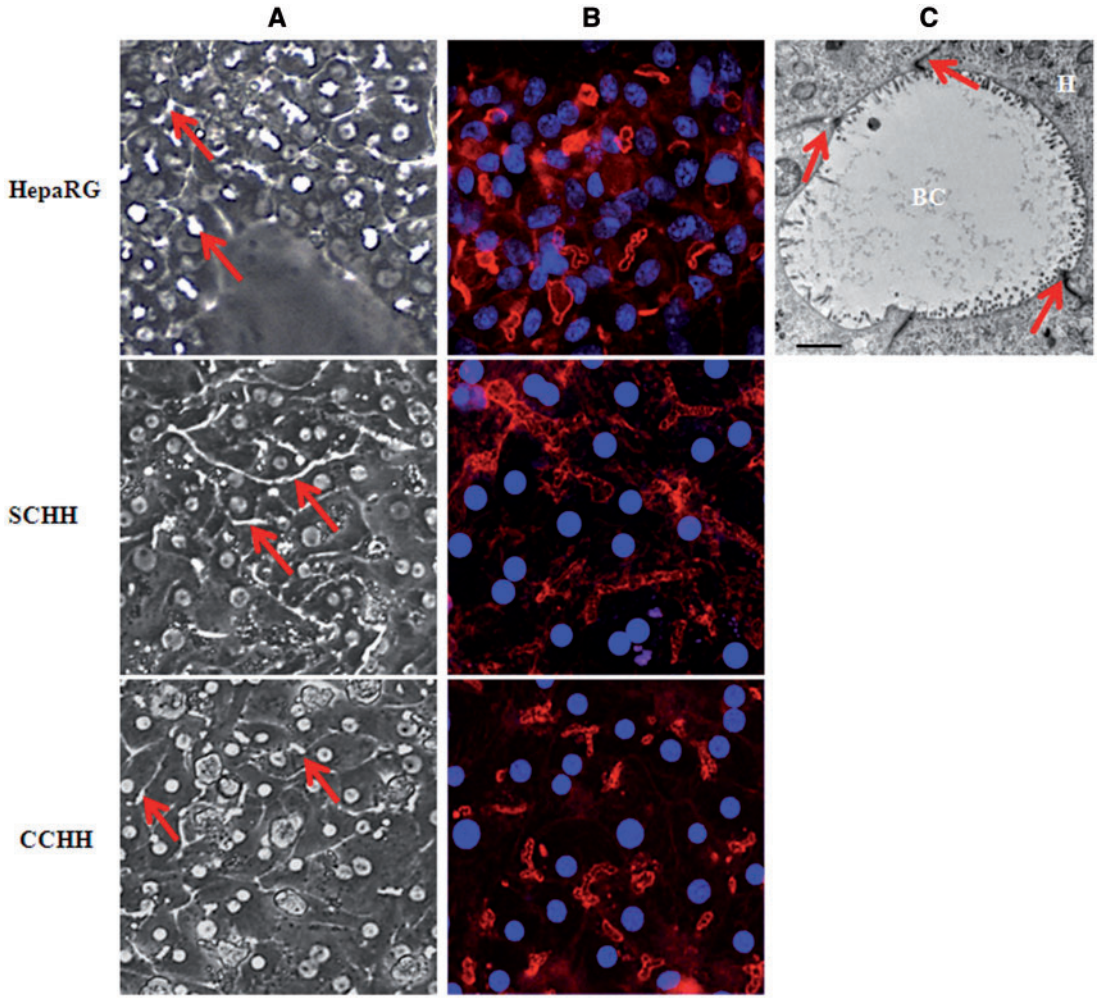

FIG. 1. Bile canaliculi networks in HepaRG cell and HH cultures. A, Bile canaliculi structures (arrows) in differentiated HepaRG cells and 4–5 days HHs cultured in sandwich (SCHH) and conventional (CCHH) configuration were observed under phase-contrast microscopy (×20 magnification). B, Pericanalicular F-actin microfilament network after labeling with phalloidin-fluoprobe in HepaRG cells (nuclei stained in using Hoechst dye) and 4–5 days HHs cultured in sandwich and conventional configuration. Imaging was done using Cellomics ArrayScan VTI HCS Reader (ThermoScientific). C, Electron microscopic micrograph of tight junctions surrounding bile canaliculus structures in HepaRG cells (arrows), original magnification × 3000 (bar = 2 μm). H, hepatocyte; BC, bile canaliculus.

Polarity of the different hepatocyte models was analyzed by phalloidin fluoprobe labeling of cytoskeletal F-actin. Labeling was particularly abundant in the pericanalicular areas which defined multiple shapes of bile canaliculi in primary hepatocytes. In SCHHs, these structures showed a time-dependent progression in the formation of a branched bile canalicular network and were more elongated than in corresponding CCHHs, especially after 4–5 days (Fig. 1B). HepaRG cells also showed abundant pericanalicular cytoskeletal F-actin and sparse network of microfilaments beneath the plasma membrane defining the cell shape. At the electron microscopic level, bile canaliculi appeared to be surrounded by large tight junctional complexes in HepaRG hepatocytes (Fig. 1C). Accordingly, the mean surface of bile canaliculi networks was estimated by measuring CDF-labeled lumen surfaces using vHCS.scan (V6.2.0) cellomics software and found to be 1.7 - and 1.3-fold higher in SCHHs than in HepaRG cells and CCHHs, respectively (Fig. 2).

Moreover, dynamics of bile canaliculi was assessed by time-lapse imaging, which allowed to analyze living cells directly over time. Some bile canaliculi showed contractions and relaxations in HepaRG cells, indicating that they were active and periodically clearing accumulated products. No synchronism was observed, even within a hepatocyte cluster (Fig. 3A). Such contractions and relaxations were slower in CCHHs (Fig. 3B) and difficult to visualize in SCHHs, likely due to the elongated shape of bile canaliculi and the upper matrigel layer.

Cellular Localization of Bile Acid Transporters

Localization of several main hepatobiliary transporters was assessed by immunofluorescence staining in HepaRG cells as well as in 4–5 days SCHHs and CCHHs. Importantly, in HepaRG cell cultures transporter immunolabeling was restricted to hepatocyte-like cells; no transporter was visualized in primitive biliary cells.

Influx Transporter

NTCP was localized to the sinusoidal membrane domain in CCHHs and SCHHs. However, immunolabeling was weaker in the former. Similarly to SCHHs, HepaRG cells showed a faint sinusoidal membrane staining and in addition a diffuse intracytoplasmic labeling for NTCP (Fig. 4).

Efflux Transporters

Basolateral domain. MRP3 was exclusively localized to the sinusoidal plasma membrane domain in all the liver cell models with a more intense labeling in HepaRG cells (Fig. 4).

Canalicular domain. Four canalicular transporters, BSEP, MRP2, MDR1, and MDR3, were immunolocalized in HHs and HepaRG cells (Fig. 4). In HHs, BSEP co-localized with cytoskeletal F-actin and was detected on canalicular membranes. It displayed a faint canalicular immunolabeling in HepaRG cells with in addition, a slight heterogeneous intracytoplasmic labeling (Supplementary Fig. 1). The other canalicular transporters, MRP2, MDR1, and MDR3, were well visualized, exclusively on canalicular membranes in the three liver cell models, with a more intense labeling of MRP2 and MDR1 in HepaRG cells (Fig. 4).

Transporter Activities

Sodium-dependent activity of NTCP. To assess whether the influx of TCA was sodium-dependent, HepaRG cells and HHs were incubated for 30 min with [^{3}H]-TCA in the presence or absence of sodium ions. Accumulation of radiolabeled TCA in cellular layers was then measured. Uptake of TCA by HepaRG cells was more than 42-fold greater in the presence of sodium demonstrating that NTCP displayed a sodium-dependent activity as in the *in vivo* situation (Fig. 5A). It was 33 and 15 times greater in presence of sodium in SCHHs and CCHHs, respectively. When measured per hepatocyte NTCP activity was around 2.2 - and 1.4-fold higher in SCHHs and CCHHs than in HepaRG cells, respectively (Fig. 5B).

Activity of efflux transporters. Efflux of CDF and [^{3}H]-TCA, substrates of MRP2 and BSEP, respectively, was assessed in standard and Ca^{2+}- and Mg^{2+}-free buffer. After 30 min incubation with CDFDA in standard buffer, fluorescent CDF was visualized in bile canaliculi of both HepaRG cells and 4–5 days SCHHs and CCHHs (Figs. 2 and 6). In contrast, absence of sharp canalicular labeling was noticed in Ca^{2+}- and Mg^{2+}-free buffer, particularly in SCHHs. Although many bile canaliculi were still labeled in HepaRG cells despite the depletion in divalent cations, the total number of fluorescent canaliculi was clearly reduced. No well-defined canalicular labeling was observed when incubation was performed in the presence of MK571, an inhibitor of MRP2 and the two other major ABC transporters MDR1 and BCRP (Matsson *et al.*, 2009).

Canalicular excretion of taurocholate was first quantified using BEI values (method I). BEI of TCA represented 26.6, 70.9, and 74.2% in HepaRG cells, CCHHs, and SCHHs, respectively (Table 1). To determine the relative contribution of diffusion, and basolateral and canalicular efflux of TCA, two other modes of calculation of TCA efflux were also used based on measurement of radiolabeled TCA in cell lysates and buffers (after incubation in buffer containing or not Ca^{2+} and Mg^{2+}) at 4 and 37°C. Incubation of cells at 4°C blocked all active transport systems, thereby allowing determination of the percentage of TCA released by diffusion (passive permeability). When calculation was based on the accumulation of radiolabeled TCA in cell lysates (method II) after incubation in a buffer containing or not divalent cations, canalicular efflux, basolateral efflux and diffusion were found to contribute nearly equally to TCA release in HepaRG cells and CCHHs, whereas in SCHHs canalicular and basolateral efflux were around 6–8% higher and diffusion was 12–16% lower compared with the two other cell models (Table 1). When radiolabeled TCA was quantified in incubation buffers (method III) containing or not Ca^{2+} and Mg^{2+} a higher contribution of basolateral efflux was observed; it became the major route of TCA excretion in HepaRG cells, SCHHs and CCHHs, ie 57.6, 43, and 35%, respectively, compared with the canalicular efflux that represented 28.5, 37.9, and 26.3%, respectively. The contribution of passive permeability to total TCA excretion was clearly lower in HepaRG cells and SCHHs (13.9 and 19.1%, respectively), whereas it remained the major route in CCHHs (38.8%). Noteworthy, when basolateral efflux and diffusion values obtained from measurements in cell lysates (method II) were summed, their percentages represented 68.7, 61.5, and 69.2% of total TCA efflux in HepaRG, SCHHs, and CCHHs, respectively; those summed from measurements in buffers (method III) gave comparable percentages representing 76.1, 62.1, and 73.7%, respectively.

MDRs activity. Incubating HepaRG cells with JC-1 dye resulted in red and green cell areas in the same microscopic field (Fig. 7). The red cell areas corresponded to primitive biliary cells, which did not express MDRs, whereas green ones represented the hepatocytes, which displayed MDRs proteins across their

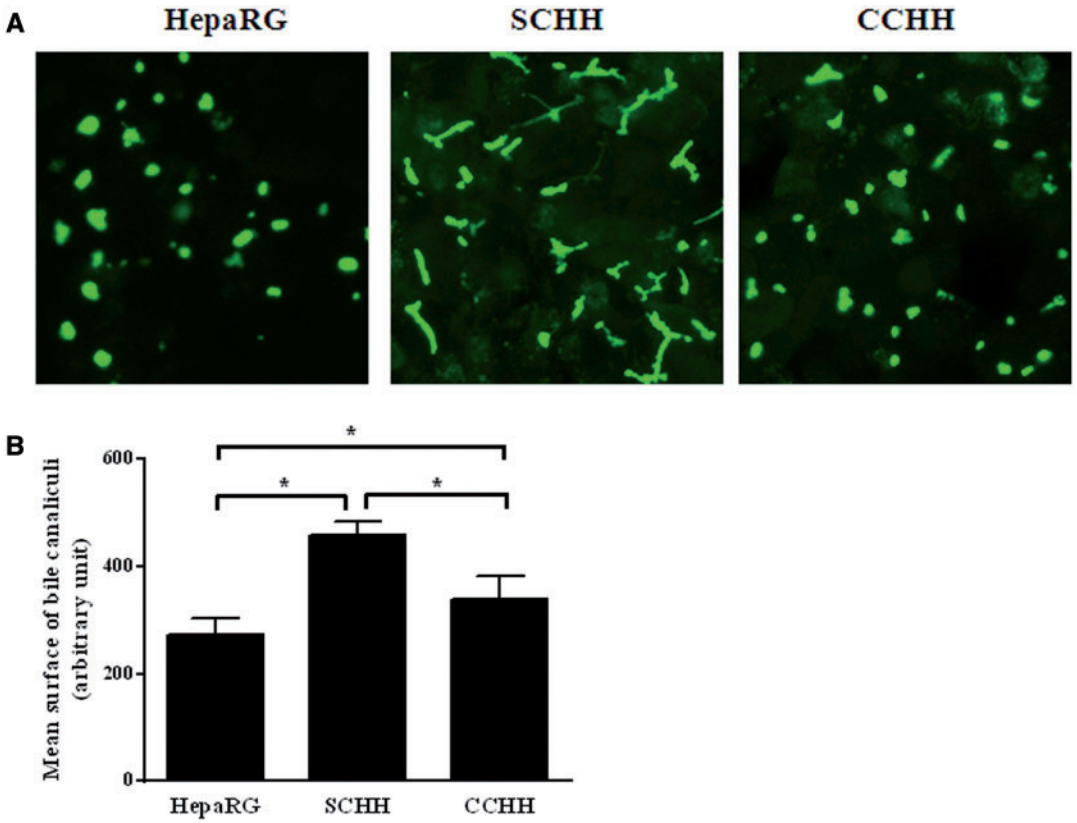

FIG. 2. Bile canaliculi networks in HepaRG cells and primary HHs. Bile canaliculi were labeled using CDFDA, a MRP2 substrate in A, HepaRG cells, SCHHs, and CCHHs. B, The mean surface areas of bile canaliculi networks in HepaRG cells and 4–5 days HHs cultured in sandwich and conventional configuration were estimated by quantifying CDFDA-labeled lumen surfaces using vHCS.scan (V6.2.0) cellomics software (ThermoScientific). Data represent the means ± SD of at least three independent experiments. Data with $P < 0.05$ is considered significant (*).

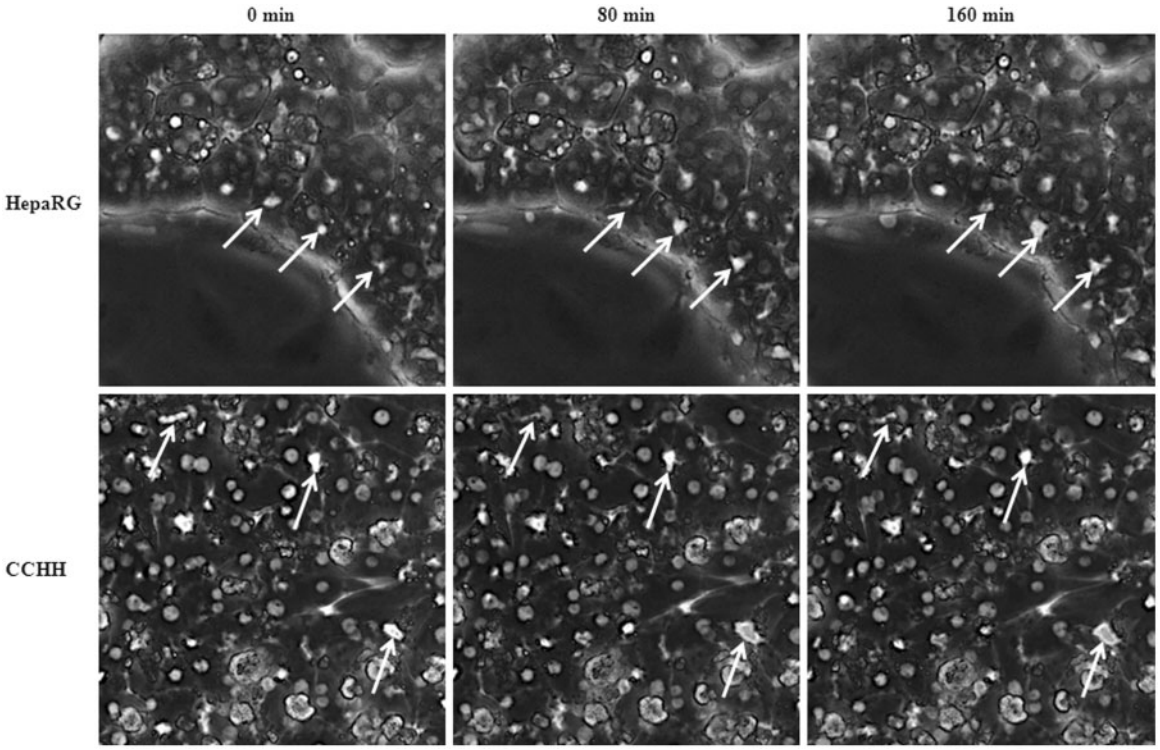

FIG. 3. Bile canaliculi dynamics in HepaRG cells and HHs. Time-lapse imaging of HepaRG cells and 4–5 days HHs cultured in conventional configuration (CCHH). Time-dependent contraction/relaxation activity of bile canaliculi (arrows). Imaging was done using inverted microscope Zeiss Axiovert 200 M and AxioCam MRm.

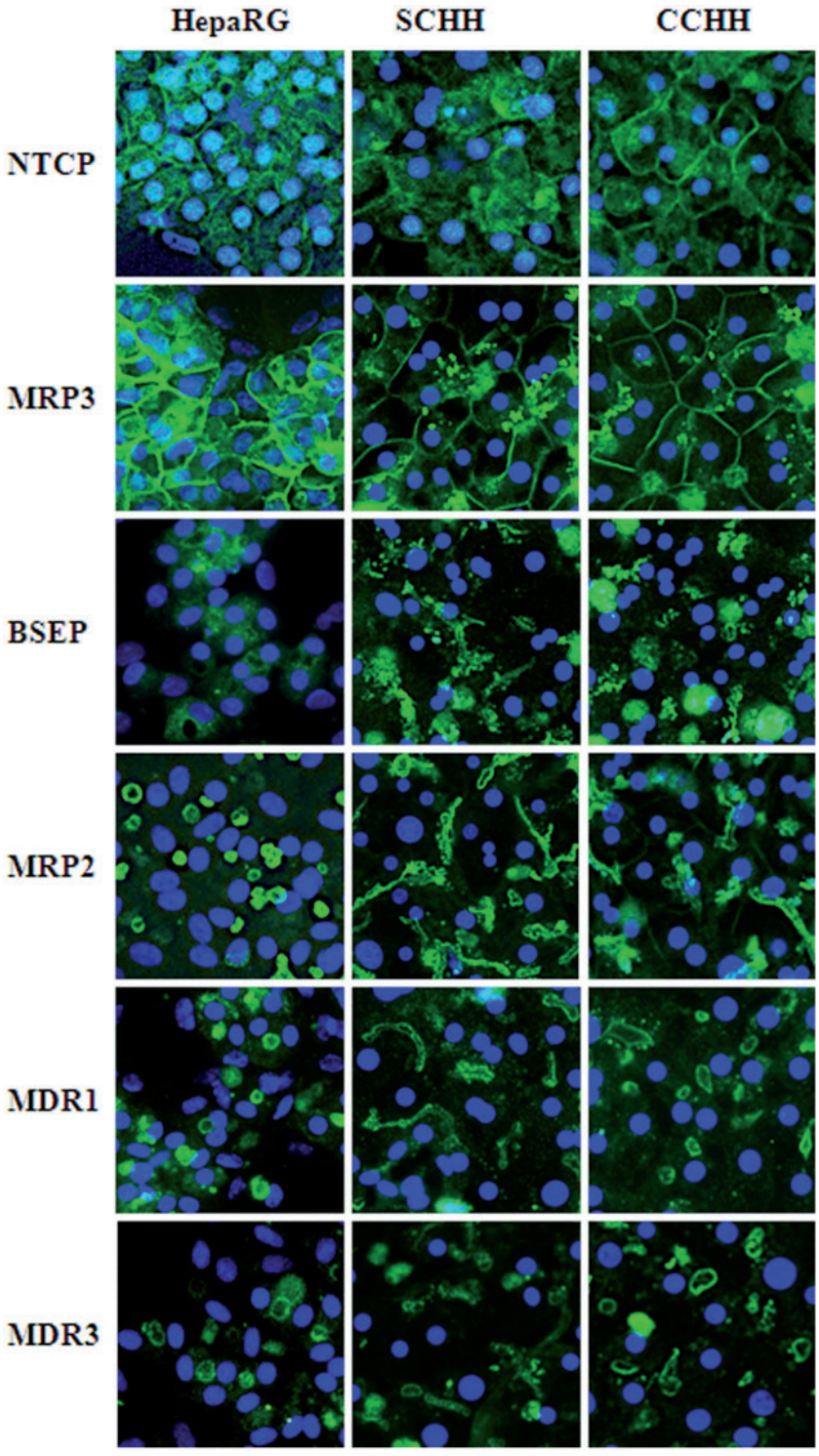

FIG. 4. Distribution of main bile acid transporters in HepaRG cells and HHs. Differentiated HepaRG cells and 4–5 days HHs in sandwich (SCHH) and conventional (CCHH) cultures were fixed and incubated with primary antibodies against each of the following hepatobiliary transporters: NTCP, MRP3, BSEP, MRP2, MDR1, and MDR3. Nuclei were labeled using Hoechst. Immunofluorescence images were obtained with a Cellomics ArrayScan VTI HCS Reader (ThermoScientific).

canalicular plasma membrane. By transporting JC-1 out of the cells, MDRs did not allow the dye to reach critical concentration to form dimers. Only pre-incubation with verapamil, an inhibitor of MDRs, before JC-1 exposure resulted in dimer fluorescence in both cell types.

DISCUSSION

Although previous studies have demonstrated that the majority of hepatobiliary transporters (organic cation transporter 1, OATP1B1, OATP2B1, NTCP, MRP2, MRP3, BSEP, and MDR1) are expressed in differentiated HepaRG cells, their distribution and

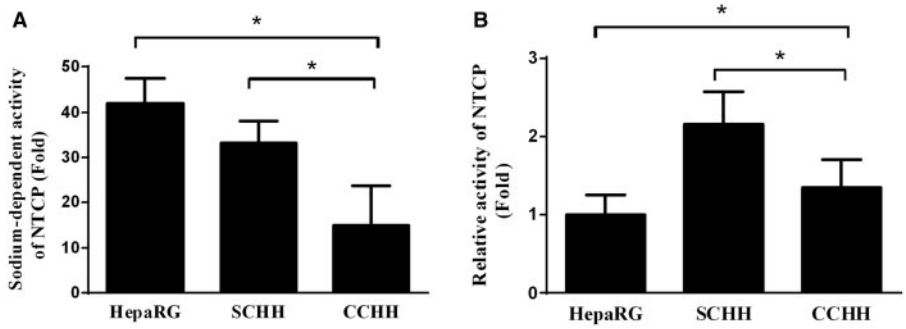

FIG. 5. Sodium-dependent activity of NTCP in HepaRG cells and HHs. HepaRG cells and 4–5 days HHs in sandwich (SCHH) and conventional (CCHH) cultures were incubated with [^{3}H]-TCA for 30 min in the presence and absence of sodium ions. A, NTCP activity was evaluated through measurement of the radiolabeled substrate TCA accumulated in cellular layers (cells plus bile canaliculi). Uptake of [^{3}H]-TCA in each cell model was expressed relative to the levels found in cells incubated with Na^+-free buffer, arbitrarily set at a value of 1. B, NTCP activity was evaluated in the presence of Na^+ as the ratio of total radioactivity measured in cell lysates to total number of hepatocytes in each cell model. Calculations were based on 800 000 hepatocytes in the two primary hepatocyte models and 280 000 HepaRG hepatocytes per well. Results are expressed relative to NTCP activity found in HepaRG hepatocytes, arbitrarily set at a value of 1. Data represent the means ± SD of at least three independent experiments. Data with $P < 0.05$ are considered significant (*).

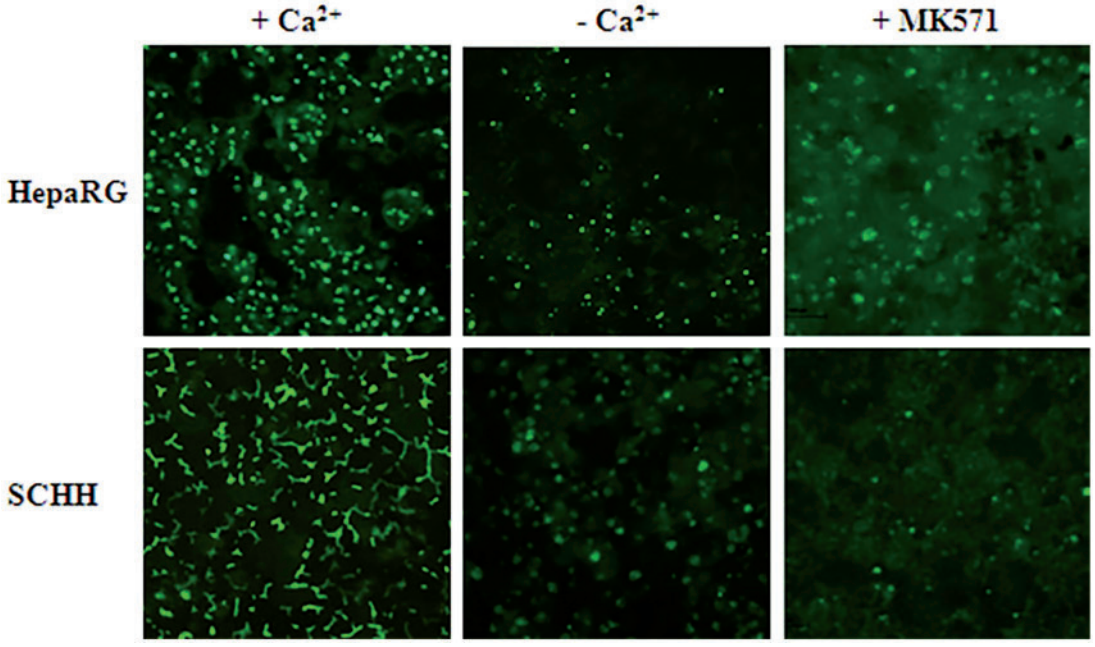

FIG. 6. Functional activity of MRP2 in HepaRG cells and HHs. MRP2 activity was estimated using CDFDA in HepaRG cells and 4–5 days SCHHs and CCHHs. Efflux of fluorescent CDF, a substrate of MRP2, characterized by accumulation of fluorescence into bile canaliculi, was evaluated in standard and Ca^{2+}- and Mg^{2+}-free buffer in the presence and absence of MK571, an inhibitor of MRP2. Imaging was done using inverted microscope Zeiss Axiovert 200 M and AxioCam MRm.

activity are still poorly documented (Anthérieu *et al.*, 2010; Kotani *et al.*, 2012; Le Vee *et al.*, 2013; Szabo *et al.*, 2013). In this study, we compared the localization and functional activity of the main membrane transporters in HepaRG cells and HHs in conventional and sandwich configuration. The major hepatobiliary transporters including BSEP and NTCP, were visualized by immunolabeling and found to be correctly distributed on canalicular and basolateral membrane domains, respectively, and to be functional in the three liver cell models. Noteworthy, primitive biliary HepaRG cells did not express detectable mRNA and protein of any tested transporter and accordingly, did not accumulate TCA (Sharanek *et al.*, 2014).

A basolateral NTCP localization together with a sodium-dependent activity (Kotani *et al.*, 2012) has been evidenced in both HepaRG cells and primary HHs. Compared to CCHHs and SCHHs, HepaRG cells showed weaker labeling and activity of NTCP which is in agreement with lower corresponding mRNA levels as previously measured in these cells compared with freshly isolated or 1-day HHs (Anthérieu *et al.*, 2012; Le Vee *et al.*, 2013). In contrast, other authors found that NTCP transcripts and protein levels were more than 2-fold higher in HepaRG cells than in cryopreserved primary HHs (Kotani *et al.*, 2012). This discrepancy likely resulted from the use of cryopreserved HHs in the latter study. Indeed, a marked reduction of protein content and activity of NTCP and other influx transporters has recently been reported in HHs associated with the freeze/thaw process (Lundquist *et al.*, 2014).

Immunolabeling of BSEP showed canalicular distribution of this transporter in HHs whatever their mode of culture, in agreement with its apical localization in human liver biopsies

and rat hepatocyte couplets (Boaglio *et al.*, 2010; Zollner *et al.*, 2001). Although much weaker than in HHs, in accordance with lower corresponding mRNA levels (Antherieu *et al.*, 2012; Le Vee *et al.*, 2013), BSEP was also detected on canalicular membranes of HepaRG cells. Moreover, noticeably, intracellular labeling was in addition observed in HepaRG cells as previously reported for rat hepatocytes *in situ* and for the WIF-B cell line (Gerloff *et al.*, 1998; Gradilone *et al.*, 2005; Soroka *et al.*, 1999). It has been emphasized that intracellular BSEP is capable of trafficking within minutes to the canalicular membrane when the demand for BSEP increased (Kipp and Arias, 2002). To our best knowledge, this study is the first immunolocalization of BSEP in HepaRG cells and primary HH cultures.

Localization of MRP2, MDR1, and MDR3 was restricted to canalicular membranes, whereas MRP3 was exclusively localized to the basolateral membrane domain in both HepaRG cells and HHs. Although no quantification was performed, immunolabeling of MRP2, MDR1, and MRP3 appeared to be more intense in HepaRG cells than in HHs, in agreement with previous studies showing overexpression of these genes at the transcriptional level in the former (Antherieu *et al.*, 2012; Le Vee *et al.*, 2013). This study provided clear evidence that the canalicular efflux transporters BSEP, MRP2, and MDRs were functional and that cholephilic substances could accumulate in bile canaliculi. BSEP and MRP2 substrates were demonstrated inside bile canaliculi of the three hepatocyte models and functional activity of MDR1 was evidenced in HepaRG hepatocytes using the JC-1 metachromatic dye of which continuous excretion by MDR1 was prevented following pre-incubation with the MDR1 inhibitor verapamil.

TABLE 1. Different Modes of Calculation of TCA Efflux in the Three Human Liver Cell Models

	HepaRG	SCHH	CCHH
BEI (%)	26.58 ± 7.26	74.15 ± 8.67*	70.94 ± 13.38*
Cell lysates			
Canalicular efflux (%)	31.26 ± 9.75	38.53 ± 15.75	30.77 ± 9.10
Basolateral efflux (%)	32.73 ± 7.34	38.05 ± 18.88	30.06 ± 1.11
Diffusion (%)	36.02 ± 6.98	23.42 ± 14.57	39.17 ± 8.37
Basolateral + diffusion (%)	68.75 ± 9.75	61.47 ± 15.75	69.23 ± 9.10
Buffers			
Canalicular efflux (%)	28.52 ± 4.77	37.86 ± 24.63	26.27 ± 9.22
Basolateral efflux (%)	57.58 ± 6.36	43.00 ± 24.16	34.95 ± 5.69
Diffusion (%)	13.89 ± 3.47	19.14 ± 11.76	38.77 ± 14.91
Basolateral + diffusion (%)	71.47 ± 6.27	62.14 ± 24.63	73.72 ± 9.22

HepaRG cells and 4–5 days SCHHs and CCHHs were exposed to [^{3}H]-TCA for 30 min to induce uptake of TCA. After 30 min incubation in standard and Ca^{2+}- and Mg^{2+}-free buffer at 4 and 37°C, TCA efflux was determined by measuring radioactivity in cell lysates and buffers. The values measured in HepaRG cells (HepaRG), and SCHHs and CCHHs are expressed as BEI or as percentages of total efflux ± SD ($n \geq 3$) and were calculated as described in 'Materials and methods' section. Conventional and sandwich cultures of fresh HHs were prepared from the same donors and analyzed in parallel. Data with $P < 0.05$ is considered significant (*).

Using other modes of calculation based on radioactivity measured in cell lysates (method II) and incubation buffers (method III) (Jemnitz *et al.*, 2010; Liu *et al.*, 1999), contribution of canalicular efflux to total excretion of TCA was found to be comparable to the BEI in HepaRG cells, representing 31.3 and 28.5%, respectively. The BEI found in this study is close to that previously reported by others (Le Vee *et al.*, 2013). Similarly, the highest values found in SCHHs were comparable to those previously obtained by Marion *et al.* (2007). However, in another study, Marion *et al.* (2012) found much lower BEI values in SCHHs. Such large differences (41.7% vs 73.2%) could reflect the well-known interindividual variations of functional activities in HHs. It has been previously reported that efflux of taurocholate was around 40–50% greater in SCHHs than in CCHHs (Kostrubsky *et al.*, 2003). The comparable BEI values found in the two primary hepatocyte models in this study could be explained by the use of fresh cells and our experimental conditions, including the type of culture medium and the choice of 4–5 days of culture before analysis of bile acid excretion. At that time, primary HHs express high levels of drug metabolizing enzymes activities and other functions (Abdel-Razzak *et al.*, 1993).

The lower BEI in HepaRG cells compared with SCHHs and CCHHs could have several nonexclusive explanations. First, an attenuated NTCP and BSEP activity in comparison to HHs regardless their mode of culture. In accordance, when the amount of accumulated TCA in cell layers was calculated per hepatocyte, it was 2.2- and 1.4-fold higher in sandwich and standard cultured HHs than in HepaRG hepatocytes, respectively. Such attenuated

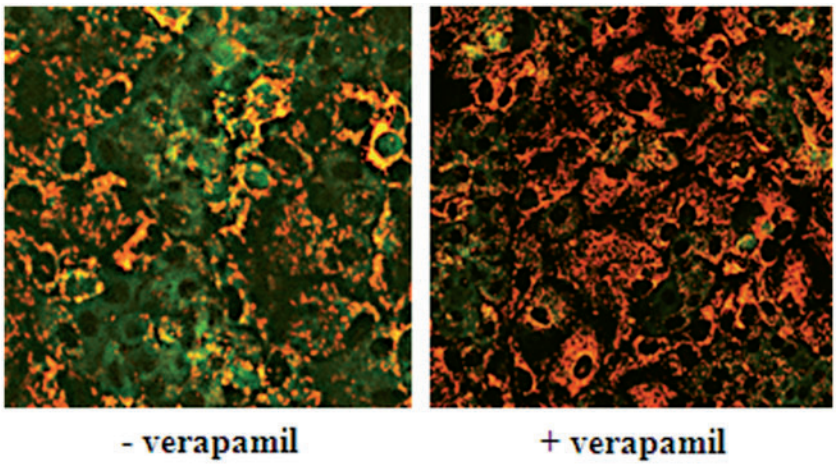

FIG. 7. MDRs activity in HepaRG cells. HepaRG cells were incubated for 30 min in the presence or absence of 50 μM verapamil, an inhibitor of MDRs, before 30 min incubation with 7 μM JC-1. A significant intracellular accumulation resulting in the formation of JC-1 dimers characterized by heterogeneous intracytoplasmic staining was observed in HepaRG hepatocytes (+ verapamil). Imaging was done using Cellomics ArrayScan VTI HCS Reader (ThermoScientific).

NTCP and BSEP activity is supported by low corresponding mRNA levels (Antherieu *et al.*, 2012; Le Vee *et al.*, 2013) and results in reduced TCA uptake and canalicular excretion. These low NTCP and BSEP activities could explain the 2.8-fold lower BEI values compared with SCHHs. Second, the overexpression of MRP3 mRNA in HepaRG cells (Antherieu *et al.*, 2012; Le Vee *et al.*, 2013) could explain the higher contribution of this route to total excretion of TCA. Third, the smaller size of the bile canaliculi network and the higher contraction/relaxation activity promoting a continuous discharge of their content. Forth, an incomplete opening of HepaRG bile canaliculi in cation-free buffer, because of the large size of tight junctions as observed under electron microscopy. This hypothesis is based on the sharp CDF-fluorescent labeling in many bile canaliculi in the absence of divalent cations in HepaRG cells, whereas such labeling was nearly completely absent in SCHHs. Noticeably, a 10–15% increase in canalicular TCA and CDF efflux was measured by using higher concentrations of the divalent cation chelator EGTA (data not shown). As a consequence, total and canalicular efflux were likely slightly underestimated in HepaRG cells.

Noteworthy, when canalicular efflux was estimated from measurement of radioactivity in either cell lysates (method II) or buffers (method III) the difference between HepaRG cells and SCHHs did not exceed 9.3% and comparable values were found in HepaRG cells and CCHHs. These limited differences between the three cell models compared with the differences in BEI values could probably be explained by the fact that the values obtained from cell lysates and buffers are based on total TCA efflux and not on TCA intracellular and bile canaliculi content (Liu *et al.*, 1999).

The contribution of passive membrane permeability was also estimated by measuring radioactivity in either cell lysates or buffers after a 30-min incubation at 4°C (Jemnitz *et al.*, 2010). High values of passive permeability reaching nearly 40% were obtained with CCHHs (in both lysates and buffers) and with HepaRG cells (cell lysates), whereas these values were much lower in SCHHs (in both lysates and buffers representing 19.1 and 23.4%, respectively) and in HepaRG cells (in buffers representing 19.1%). Moreover, large interassay variations were apparent in the two HH models. Noticeably, around 30% diffusion was also reported with rat hepatocytes which have a higher basolateral efflux activity than HHs (Jemnitz *et al.*, 2010). All these data lead to the conclusion that the experimental conditions used to evaluate passive permeability may result in its overestimation. This could at least partly be due to excessive release of TCA, for instance during cell detachment from the culture dishes. Obviously, analysis of passive permeability in the three liver cell models deserves further investigations.

In conclusion, this study demonstrated that HepaRG hepatocytes displayed a set of main hepatobiliary transporter proteins (NTCP, MRP3, BSEP, MRP2, MDR1, and MDR3) at the appropriate membrane domains and all the tested ones (NTCP, BSEP, and MDRs) were functional as in primary HHs. To our best knowledge, this work is the first comparative localization and functional activity evaluation of the main membrane transporters in HepaRG cells and primary HHs. Analysis of basolateral and canalicular TCA efflux showed that the excretion mode of TCA was comparable in both cell models. However, some quantitative differences in relative canalicular and basolateral efflux were observed; they could be explained not only by variations in the levels of NTCP, BSEP, and basolateral efflux transporters but also by the size of the bile canaliculi network and its constriction/relaxation activity. HepaRG hepatocytes have already shown their unique interest for analyzing bile canaliculi function and response to cholestatic agents (Antherieu *et al.*, 2013; Bachour-El Azzi *et al.*, 2014; Sharanek *et al.*, 2014). The data reported in this study bring further information on mechanisms by which bile acids can accumulate and be excreted in either HepaRG cells or primary hepatocytes. Altogether our data support the conclusion that with the advantages to be a reproducible and easy to handle cell model, HepaRG hepatocytes represent a unique model for investigating hepatobiliary transport and xenobiotic effects on canalicular efflux and cholestasis–induced features.

SUPPLEMENTARY DATA

Supplementary data are available online at http://toxsci.oxfordjournals.org/.

FUNDING

The Lebanese University, Lebanese National Council for Scientific Research (to P.B.E.); Philippe Jabre association (to P.B.E.); the Doctorate School vie-agro-santé Rennes (to P.B.E.); Lebanese Association for Scientific Research (to A.S.); the French-Lebanon Cèdre program 11 S F47/L2 (2011–2012); and the European Community (Contracts Predict-IV-202222 and MIP-DILI-115336). The MIP-DILI project has received support from the Innovative Medicines Initiative Joint Undertaking, resources of which are composed of financial contribution from the European Union's Seventh Framework Programme (FP7/20072013) and EFPIA companies' in kind contribution. http://www.imi.europa.eu/.

REFERENCES

Abdel-Razzak, Z., Loyer, P., Fautrel, A., Gautier, J. C., Corcos, L., Turlin, B., Beaune, P., and Guillouzo, A. (1993). Cytokines down-regulate expression of major cytochrome P-450 enzymes in adult human hepatocytes in primary culture. *Mol. Pharmacol.* **44,** 707–715.

Antherieu, S., Bachour-El Azzi, P., Dumont, J., Abdel-Razzak, Z., Guguen-Guillouzo, C., Fromenty, B., Robin, M. A., and Guillouzo, A. (2013). Oxidative stress plays a major role in chlorpromazine-induced cholestasis in human HepaRG cells. *Hepatology* **57,** 1518–1529.

Antherieu, S., Chesne, C., Li, R., Camus, S., Lahoz, A., Picazo, L., Turpeinen, M., Tolonen, A., Uusitalo, J., Guguen-Guillouzo, C., *et al.* (2010). Stable expression, activity, and inducibility of cytochromes P450 in differentiated HepaRG cells. *Drug Metab. Dispos.* **38,** 516–525.

Antherieu, S., Chesne, C., Li, R., Guguen-Guillouzo, C., and Guillouzo, A. (2012). Optimization of the HepaRG cell model for drug metabolism and toxicity studies. *Toxicol. In Vitro* **26,** 1278–1285.

Bachour-El Azzi, P., Sharanek, A., Abdel-Razzak, Z., Antherieu, S., Al-Attrache, H., Savary, C. C., Lepage, S., Morel, I., Labbe, G., Guguen-Guillouzo, C., *et al.* (2014). Impact of inflammation on chlorpromazine-induced cytotoxicity and cholestatic features in HepaRG cells. *Drug Metab. Dispos.* **42,** 1556–1566.

Boaglio, A. C., Zucchetti, A. E., Sanchez Pozzi, E. J., Pellegrino, J. M., Ochoa, J. E., Mottino, A. D., Vore, M., Crocenzi, F. A., and Roma, M. G. (2010). Phosphoinositide 3-kinase/protein kinase B signaling pathway is involved in estradiol

17beta-D-glucuronide-induced cholestasis: Complementarity with classical protein kinase C. *Hepatology* **52,** 1465–1476.

Cerec, V., Glaise, D., Garnier, D., Morosan, S., Turlin, B., Drenou, B., Gripon, P., Kremsdorf, D., Guguen-Guillouzo, C., and Corlu, A. (2007). Transdifferentiation of hepatocyte-like cells from the human hepatoma HepaRG cell line through bipotent progenitor. *Hepatology* **45,** 957–967.

Copple, B. L., Jaeschke, H., and Klaassen, C. D. (2010). Oxidative stress and the pathogenesis of cholestasis. *Semin. Liver Dis.* **30,** 195–204.

Corsini, A., and Bortolini, M. (2013). Drug-induced liver injury: The role of drug metabolism and transport. *J. Clin. Pharmacol.* **53,** 463–474.

De Bruyn, T., Chatterjee, S., Fattah, S., Keemink, J., Nicolai, J., Augustijns, P., and Annaert, P. (2013). Sandwich-cultured hepatocytes: Utility for in vitro exploration of hepatobiliary drug disposition and drug-induced hepatotoxicity. *Expert Opin. Drug Metab. Toxicol.* **9,** 589–616.

Gerloff, T., Stieger, B., Hagenbuch, B., Madon, J., Landmann, L., Roth, J., Hofmann, A. F., and Meier, P. J. (1998). The sister of P-glycoprotein represents the canalicular bile salt export pump of mammalian liver. *J. Biol. Chem.* **273,** 10046–10050.

Gradilone, S. A., Tietz, P. S., Splinter, P. L., Marinelli, R. A., and LaRusso, N. F. (2005). Expression and subcellular localization of aquaporin water channels in the polarized hepatocyte cell line, WIF-B. *BMC Physiol.* **5,** 13.

Guguen-Guillouzo, C., and Guillouzo, A. (2010). General review on in vitro hepatocyte models and their applications. *Methods Mol. Biol.* **640,** 1–40.

Giacomini, K. M., Huang, S. M., Tweedie, D. J., Benet, L. Z., Brouwer, K. L., Chu, X., Dahlin, A., Evers, R., Fischer, V., Hillgren, K. M., Hoffmaster, K. A., Ishikawa, T., Keppler, D., Kim, R. B., Lee, C. A., Niemi, M., Polli, J. W., Sugiyama, Y., Swaan, P. W., Ware, J. A., Wright, S. H., Yee, S. W., Zamek-Gliszczynski, M. J., and Zhang, L. (2010). International Transporter Consortium. Membrane transporters in drug development. *Nat. Rev. Drug Discov.* **9,** 215–236.

Guguen-Guillouzo, C., Campion, J. P., Brissot, P., Glaise, D., Launois, B., Bourel, M., and Guillouzo, A. (1982). High yield preparation of isolated human adult hepatocytes by enzymatic perfusion of the liver. *Cell Biol. Int. Rep.* **6,** 625–628.

Hofmann, A. F. (1999). Bile acids: The good, the bad, and the ugly. *News Physiol. Sci.* **14,** 24–29.

Jemnitz, K., Veres, Z., and Vereczkey, L. (2010). Contribution of high basolateral bile salt efflux to the lack of hepatotoxicity in rat in response to drugs inducing cholestasis in human. *Toxicol. Sci.* **115,** 80–88.

Kipp, H., and Arias, I. M. (2002). Trafficking of canalicular ABC transporters in hepatocytes. *Annu. Rev. Physiol.* **64,** 595–608.

Kostrubsky, V. E., Strom, S. C., Hanson, J., Urda, E., Rose, K., Burliegh, J., Zocharski, P., Cai, H., Sinclair, J. F., and Sahi, J. (2003). Evaluation of hepatotoxic potential of drugs by inhibition of bile-acid transport in cultured primary human hepatocytes and intact rats. *Toxicol. Sci.* **76,** 220–228.

Kotani, N., Maeda, K., Debori, Y., Camus, S., Li, R., Chesne, C., and Sugiyama, Y. (2012). Expression and transport function of drug uptake transporters in differentiated HepaRG cells. *Mol. Pharm.* **9,** 3434–3441.

Kullak-Ublick, G. A., Glasa, J., Boker, C., Oswald, M., Grutzner, U., Hagenbuch, B., Stieger, B., Meier, P. J., Beuers, U., Kramer, W., *et al.* (1997). Chlorambucil-taurocholate is transported by bile acid carriers expressed in human hepatocellular carcinomas. *Gastroenterology* **113,** 1295–1305.

Kullak-Ublick, G. A., Stieger, B., Hagenbuch, B., and Meier, P. J. (2000). Hepatic transport of bile salts. *Semin. Liver Dis.* **20,** 273–292.

Le Vee, M., Noel, G., Jouan, E., Stieger, B., and Fardel, O. (2013). Polarized expression of drug transporters in differentiated human hepatoma HepaRG cells. *Toxicol. In Vitro* **27,** 1979–1986.

Lefebvre, P., Cariou, B., Lien, F., Kuipers, F., and Staels, B. (2009). Role of bile acids and bile acid receptors in metabolic regulation. *Physiol. Rev.* **89,** 147–191.

Legrand, O., Perrot, J. Y., Simonin, G., Baudard, M., and Marie, J. P. (2001). JC-1: A very sensitive fluorescent probe to test Pgp activity in adult acute myeloid leukemia. *Blood* **97,** 502–508.

Liu, J., Lu, H., Lu, Y. F., Lei, X., Cui, J. Y., Ellis, E., Strom, S. C., and Klaassen, C. D. (2014). Potency of individual bile acids to regulate bile acid synthesis and transport genes in primary human hepatocyte cultures. *Toxicol. Sci.* **141,** 538–546.

Liu, X., LeCluyse, E. L., Brouwer, K. R., Gan, L. S., Lemasters, J. J., Stieger, B., Meier, P. J., and Brouwer, K. L. (1999). Biliary excretion in primary rat hepatocytes cultured in a collagen-sandwich configuration. *Am. J. Physiol.* **277,** 12–21.

Lundquist, P., Loof, J., Sohlenius-Sternbeck, A. K., Floby, E., Johansson, J., Bylund, J., Hoogstraate, J., Afzelius, L., and Andersson, T. B. (2014). The impact of solute carrier (SLC) drug uptake transporter loss in human and rat cryopreserved hepatocytes on clearance predictions. *Drug Metab. Dispos.* **42,** 469–480.

Marion, T. L., Leslie, E. M., and Brouwer, K. L. (2007). Use of sandwich-cultured hepatocytes to evaluate impaired bile acid transport as a mechanism of drug-induced hepatotoxicity. *Mol. Pharm.* **4,** 911–918.

Marion, T. L., Perry, C. H., St Claire, R. L., 3rd, and Brouwer, K. L. (2012). Endogenous bile acid disposition in rat and human sandwich-cultured hepatocytes. *Toxicol. Appl. Pharmacol.* **261,** 1–9.

Matsson, P., Pedersen, J. M., Norinder, U., Bergstrom, C. A., and Artursson, P. (2009). Identification of novel specific and general inhibitors of the three major human ATP-binding cassette transporters P-gp, BCRP and MRP2 among registered drugs. *Pharm. Res.* **26,** 1816–1831.

Meier, P. J., and Stieger, B. (2002). Bile salt transporters. *Annu. Rev. Physiol.* **64,** 635–661.

Nathanson, M. H., and Boyer, J. L. (1991). Mechanisms and regulation of bile secretion. *Hepatology* **14,** 551–566.

Noe, J., Stieger, B., and Meier, P. J. (2002). Functional expression of the canalicular bile salt export pump of human liver. *Gastroenterology* **123,** 1659–1666.

Pauli-Magnus, C., Meier, P. J., and Stieger, B. (2010). Genetic determinants of drug-induced cholestasis and intrahepatic cholestasis of pregnancy. *Semin. Liver Dis.* **30,** 147–159.

Perez, L. M., Milkiewicz, P., Elias, E., Coleman, R., Sanchez Pozzi, E. J., and Roma, M. G. (2006). Oxidative stress induces internalization of the bile salt export pump, Bsep, and bile salt secretory failure in isolated rat hepatocyte couplets: A role for protein kinase C and prevention by protein kinase A. *Toxicol. Sci.* **91,** 150–158.

Pernelle, K., Le Guevel, R., Glaise, D., Stasio, C. G., Le Charpentier, T., Bouaita, B., Corlu, A., and Guguen-Guillouzo, C. (2011). Automated detection of hepatotoxic compounds in human hepatocytes using HepaRG cells and image-based analysis of mitochondrial dysfunction with JC-1 dye. *Toxicol. Appl. Pharmacol.* **254,** 256–266.

Roma, M. G., and Sanchez Pozzi, E. J. (2008). Oxidative stress: A radical way to stop making bile. *Ann. Hepatol.* **7,** 16–33.

Sharanek, A., Azzi, P. B., Al-Attrache, H., Savary, C. C., Humbert, L., Rainteau, D., Guguen-Guillouzo, C., and Guillouzo, A. (2014). Different dose-dependent mechanisms are involved in early cyclosporine a-induced cholestatic effects in hepaRG cells. *Toxicol. Sci.* **141,** 244–253.

Soroka, C. J., Pate, M. K., and Boyer, J. L. (1999). Canalicular export pumps traffic with polymeric immunoglobulin A receptor on the same microtubule-associated vesicle in rat liver. *J. Biol. Chem.* **274,** 26416–26424.

Swift, B., Pfeifer, N. D., and Brouwer, K. L. (2010). Sandwich-cultured hepatocytes: An in vitro model to evaluate hepatobiliary transporter-based drug interactions and hepatotoxicity. *Drug Metab. Rev.* **42,** 446–471.

Szabo, M., Veres, Z., Baranyai, Z., Jakab, F., and Jemnitz, K. (2013). Comparison of human hepatoma HepaRG cells with human and rat hepatocytes in uptake transport assays in order to predict a risk of drug induced hepatotoxicity. *PLoS One* **8,** e59432.

Trauner, M., and Boyer, J. L. (2003). Bile salt transporters: Molecular characterization, function, and regulation. *Physiol. Rev.* **83,** 633–671.

Trauner, M., Meier, P. J., and Boyer, J. L. (1998). Molecular pathogenesis of cholestasis. *N. Engl. J. Med.* **339,** 1217–1227.

Zamek-Gliszczynski, M. J., Xiong, H., Patel, N. J., Turncliff, R. Z., Pollack, G. M., and Brouwer, K. L. (2003). Pharmacokinetics of 5 (and 6)-carboxy-2',7'-dichlorofluorescein and its diacetate promoiety in the liver. *J. Pharmacol. Exp. Ther.* **304,** 801–809.

Zollner, G., Fickert, P., Zenz, R., Fuchsbichler, A., Stumptner, C., Kenner, L., Ferenci, P., Stauber, R. E., Krejs, G. J., Denk, H., *et al.* (2001). Hepatobiliary transporter expression in percutaneous liver biopsies of patients with cholestatic liver diseases. *Hepatology* **33,** 633–646.